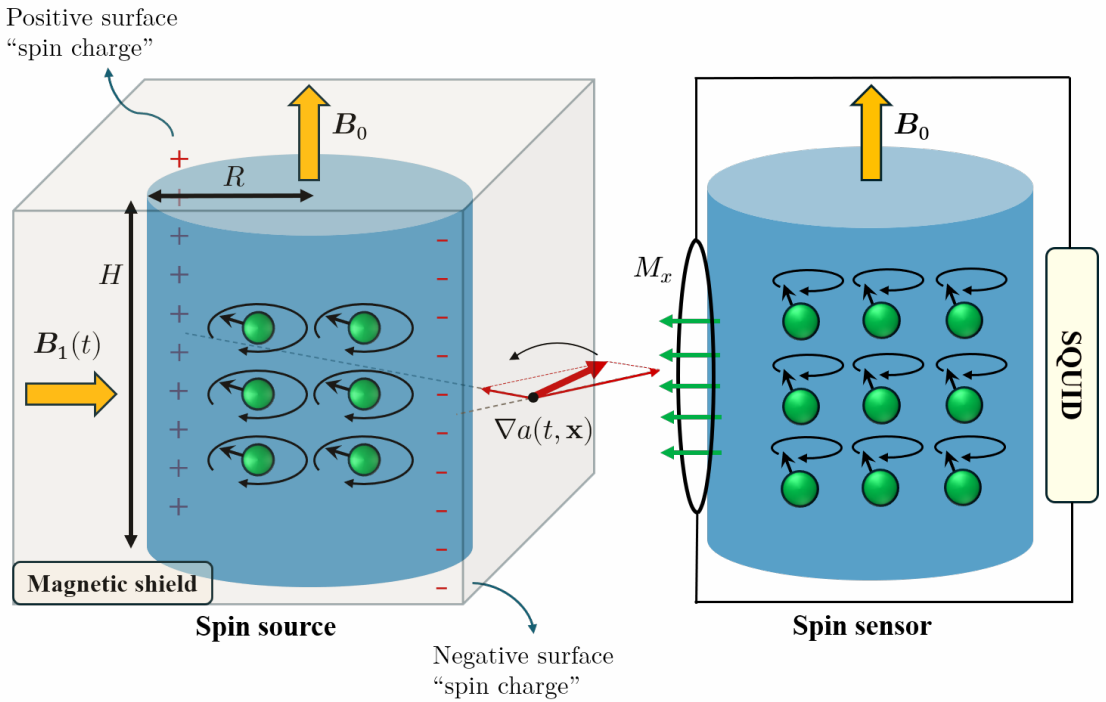

Axion Production and Detection Using a Dual NMR-type Experiment

Qiushi Wei

Based on 2510.18944
In collaboration with Jeff A. Dror and Fengwei Yang

UF | Physics

Φαινό 2026
The 2026 Phenomenology Symposium

The Axion

- Solves the strong CP problem
- Can be dark matter
- Mostly searched for via axion-photon coupling ($g_{a\gamma\gamma} a \mathbf{E} \cdot \mathbf{B}$) and axion-nucleon coupling ($g_{aN} \partial_\mu a \bar{N} \gamma^\mu \gamma^5 N$ ...)

The Axion

- Solves the strong CP problem
- Can be dark matter
- Mostly searched for via axion-photon coupling ($g_{a\gamma\gamma} a \mathbf{E} \cdot \mathbf{B}$) and axion-nucleon coupling ($g_{aN} \partial_\mu a \bar{N} \gamma^\mu \gamma^5 N$ ...)

Assuming axion dark matter:

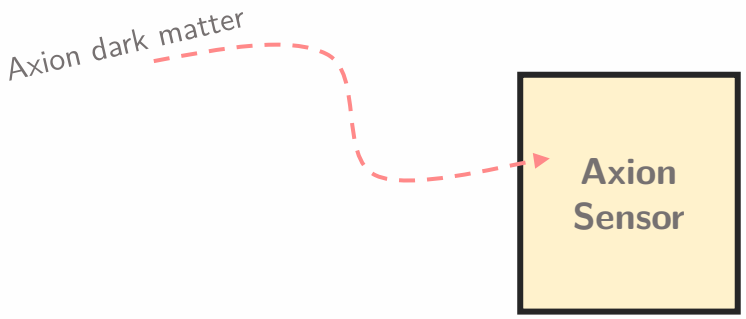

Eg. ADMX, CASPEr

Not assuming axion dark matter:

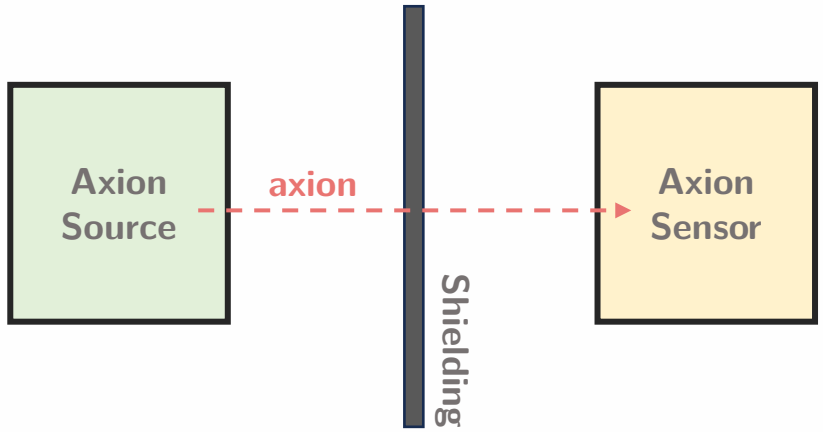

Eg. Light-shining-through-walls, ARIADNE

The Axion

- Solves the strong CP problem
- Can be dark matter
- Mostly searched for via axion-photon coupling ($g_{a\gamma\gamma} a \mathbf{E} \cdot \mathbf{B}$) and axion-nucleon coupling ($g_{aN} \partial_\mu a \bar{N} \gamma^\mu \gamma^5 N$ ...)

Assuming axion dark matter:

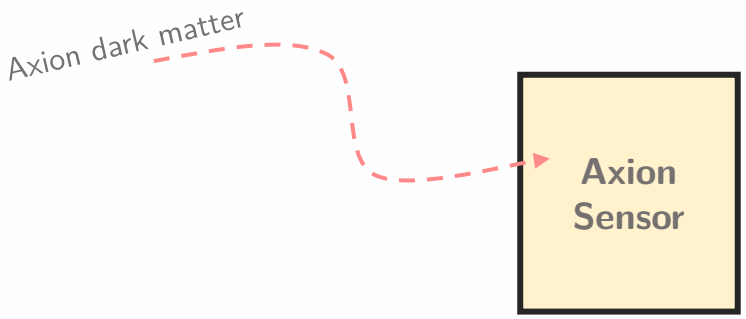

Eg. ADMX, CASPEr

Not assuming axion dark matter:

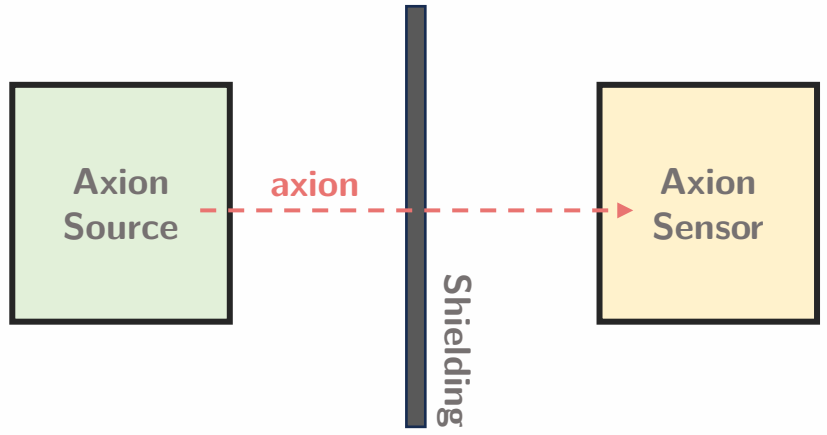

Eg. Light-shining-through-walls, ARIADNE

Can we both produce and detect axions with axion-nucleon coupling?

$$\mathcal{L} \supset g_{aN} \partial_\mu a \bar{N} \gamma^\mu \gamma^5 N$$

Can we both produce and detect axions with axion-nucleon coupling?

$$\mathcal{L} \supset g_{aN} \partial_\mu a \bar{N} \gamma^\mu \gamma^5 N$$

For a spin-1/2 non-relativistic nucleus

$$H_{\text{int}} = -2 g_{aN} \nabla a(t, \mathbf{x}) \cdot \mathbf{S}$$

$$\mathbf{B}_a(t, \mathbf{x}) = \frac{2 g_{aN}}{\gamma} \nabla a(t, \mathbf{x})$$

Zeeman effect:

$$H_{\text{Zeeman}} = -\boldsymbol{\mu} \cdot \mathbf{B}$$

$$\boldsymbol{\mu} = \gamma \mathbf{S}$$

Can we both produce and detect axions with axion-nucleon coupling?

$$\mathcal{L} \supset g_{aN} \partial_\mu a \bar{N} \gamma^\mu \gamma^5 N$$

For a spin-1/2 non-relativistic nucleus

$$H_{\text{int}} = -2 g_{aN} \nabla a(t, \mathbf{x}) \cdot \mathbf{S}$$

$$\mathbf{B}_a(t, \mathbf{x}) = \frac{2 g_{aN}}{\gamma} \nabla a(t, \mathbf{x})$$

Zeeman effect:

$$H_{\text{Zeeman}} = -\boldsymbol{\mu} \cdot \mathbf{B}$$

$$\boldsymbol{\mu} = \gamma \mathbf{S}$$

"Axion-induced NMR"

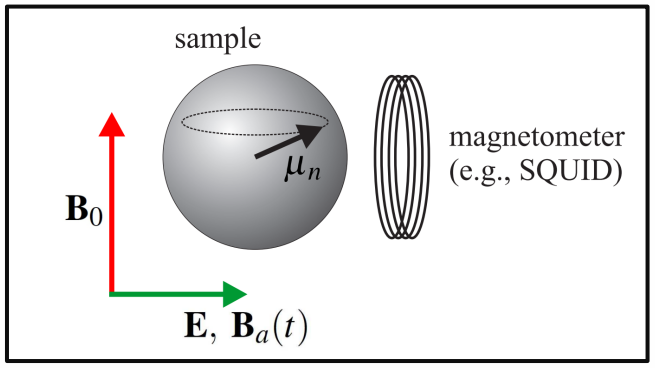

[Kimball, et al. (CASPEr) – 2018]

Can we both produce and detect axions with axion-nucleon coupling?

$$\mathcal{L} \supset g_{aN} \partial_\mu a \bar{N} \gamma^\mu \gamma^5 N$$

For axions

$$(\partial_t^2 - \nabla^2 + m_a^2) a(t, \mathbf{x}) = 2 g_{aN} \nabla \cdot \mathbf{s}(t, \mathbf{x})$$

Nuclear spin density
(NR, spin-1/2)

For a spin-1/2 non-relativistic nucleus

$$H_{\text{int}} = -2 g_{aN} \nabla a(t, \mathbf{x}) \cdot \mathbf{S}$$

$$\mathbf{B}_a(t, \mathbf{x}) = \frac{2 g_{aN}}{\gamma} \nabla a(t, \mathbf{x})$$

Zeeman effect:

$$H_{\text{Zeeman}} = -\boldsymbol{\mu} \cdot \mathbf{B}$$

$$\boldsymbol{\mu} = \gamma \mathbf{S}$$

"Axion-induced NMR"

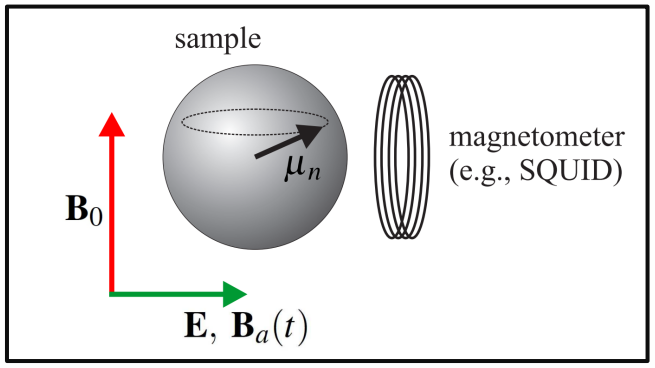

[Kimball, et al. (CASPEr) – 2018]

Can we both produce and detect axions with axion-nucleon coupling?

$$\mathcal{L} \supset g_{aN} \partial_\mu a \bar{N} \gamma^\mu \gamma^5 N$$

For axions

$$(\partial_t^2 - \nabla^2 + m_a^2) a(t, \mathbf{x}) = 2 g_{aN} \nabla \cdot \mathbf{s}(t, \mathbf{x})$$

Nuclear spin density
(NR, spin-1/2)

For a spin-1/2 non-relativistic nucleus

$$H_{\text{int}} = -2 g_{aN} \nabla a(t, \mathbf{x}) \cdot \mathbf{S}$$

$$\mathbf{B}_a(t, \mathbf{x}) = \frac{2 g_{aN}}{\gamma} \nabla a(t, \mathbf{x})$$

Zeeman effect:

$$H_{\text{Zeeman}} = -\boldsymbol{\mu} \cdot \mathbf{B}$$

$$\boldsymbol{\mu} = \gamma \mathbf{S}$$

"NMR-induced axion"

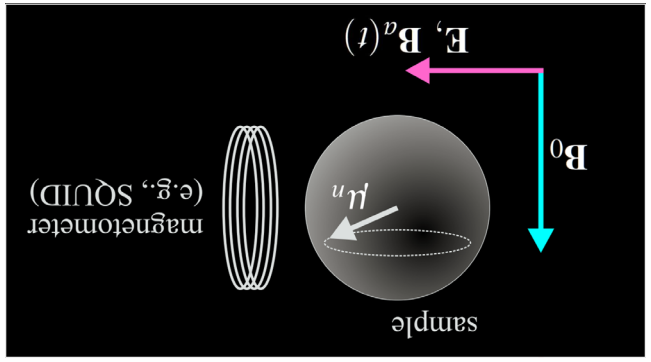

"Axion-induced NMR"

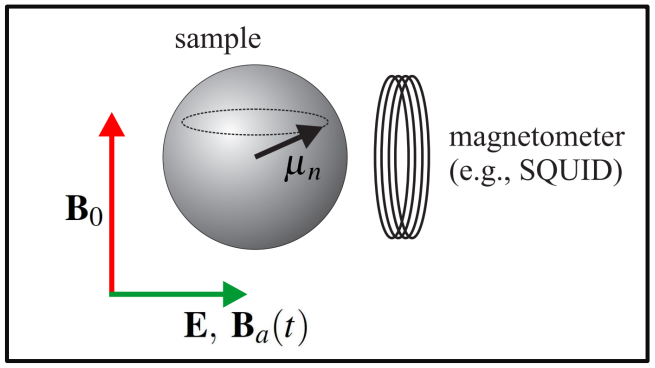

[Kimball, et al. (CASPEr) – 2018]

Can we both produce and detect axions with axion-nucleon coupling?

$$\mathcal{L} \supset g_{aN} \partial_\mu a \bar{N} \gamma^\mu \gamma^5 N$$

For axions

$$(\partial_t^2 - \nabla^2 + m_a^2) a(t, \mathbf{x}) = 2 g_{aN} \nabla \cdot \mathbf{s}(t, \mathbf{x})$$

Nuclear spin density
(NR, spin-1/2)

For a spin-1/2 non-relativistic nucleus

$$H_{\text{int}} = -2 g_{aN} \nabla a(t, \mathbf{x}) \cdot \mathbf{S}$$

$$\mathbf{B}_a(t, \mathbf{x}) = \frac{2 g_{aN}}{\gamma} \nabla a(t, \mathbf{x})$$

Zeeman effect:

$$H_{\text{Zeeman}} = -\boldsymbol{\mu} \cdot \mathbf{B}$$

$$\boldsymbol{\mu} = \gamma \mathbf{S}$$

"NMR-induced axion"

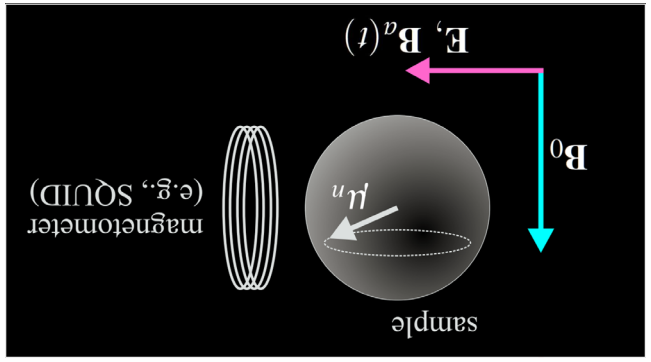

+

"Axion-induced NMR"

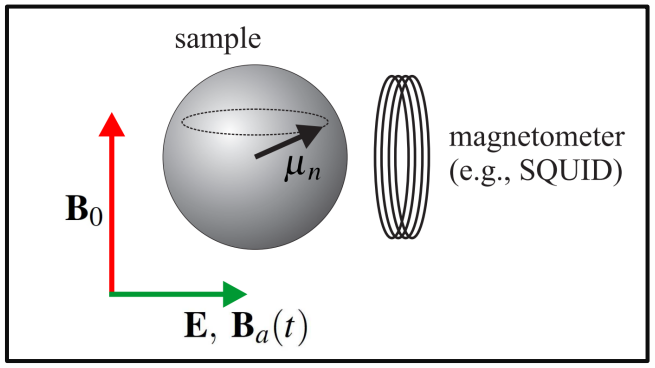

[Kimball, et al. (CASPEr) – 2018]

NMR-induced Axion

In electrodynamics: $\rho_{\rm p} = -\nabla \cdot \mathbf{P}$

- **Coherent spin-precessing source:**

$$a(t,\mathbf{x}) = g_{aN} \int d^3x' \, \frac{1}{4\pi|\mathbf{x}-\mathbf{x}'|} e^{ik_0|\mathbf{x}-\mathbf{x}'|} \rho_{\rm s}(t,\mathbf{x}')$$

$\rho_{\rm s}(t,\mathbf{x}) \equiv -2\nabla \cdot \mathbf{s}(t,\mathbf{x})$

A "spin charge" distribution induced by spin polarization

$$k_0 \equiv \begin{cases} \sqrt{\omega_0^2 - m_a^2}, & (\text{if } \omega_0 \geq m_a) \\ i\kappa_0, \ \kappa_0 \equiv \sqrt{m_a^2 - \omega_0^2} & (\text{if } \omega_0 < m_a) \end{cases}$$

$$\mathbf{s}(t,\mathbf{x}) = e^{-i\omega_0 t}\mathbf{s}(\mathbf{x}), \quad \rho_{\rm s}(t,\mathbf{x}) = e^{-i\omega_0 t}\rho_{\rm s}(\mathbf{x}), \quad a(t,\mathbf{x}) = e^{-i\omega_0 t}a(\mathbf{x})$$ (Real part as the physical quantity)

NMR-induced Axion

In electrodynamics: $\rho_{\rm p} = -\nabla \cdot \mathbf{P}$

- **Coherent spin-precessing source:**

$$a(t,\mathbf{x}) = g_{aN} \int d^3x' \, \frac{1}{4\pi|\mathbf{x}-\mathbf{x}'|} e^{ik_0|\mathbf{x}-\mathbf{x}'|} \rho_{\rm s}(t,\mathbf{x}')$$

$\rho_{\rm s}(t,\mathbf{x}) \equiv -2\nabla \cdot \mathbf{s}(t,\mathbf{x})$

A "spin charge" distribution induced by spin polarization

$$k_0 \equiv \begin{cases} \sqrt{\omega_0^2 - m_a^2}, & (\text{if } \omega_0 \geq m_a) \\ i\kappa_0, \ \kappa_0 \equiv \sqrt{m_a^2 - \omega_0^2} & (\text{if } \omega_0 < m_a) \end{cases}$$

$$\mathbf{s}(t,\mathbf{x}) = e^{-i\omega_0 t}\mathbf{s}(\mathbf{x}), \quad \rho_{\rm s}(t,\mathbf{x}) = e^{-i\omega_0 t}\rho_{\rm s}(\mathbf{x}), \quad a(t,\mathbf{x}) = e^{-i\omega_0 t}a(\mathbf{x})$$ (Real part as the physical quantity)

- **Near-Field Limit:** $k_0|\mathbf{x}-\mathbf{x}'| \ll 1$ or $\kappa_0|\mathbf{x}-\mathbf{x}'| \ll 1$ $\qquad 1\text{GHz} \times 1\text{cm} \simeq 0.03$

$$a(t,\mathbf{x}) = g_{aN} \int d^3x' \, \frac{1}{4\pi|\mathbf{x}-\mathbf{x}'|} \rho_{\rm s}(t,\mathbf{x}'), \qquad \nabla a(t,\mathbf{x}) = -g_{aN} \int d^3x' \, \frac{\mathbf{x}-\mathbf{x}'}{4\pi|\mathbf{x}-\mathbf{x}'|^3} \rho_{\rm s}(t,\mathbf{x}')$$

Analogy with electrostatics

$g_{aN} \longleftrightarrow 1/\epsilon_0, \quad a(t,\mathbf{x}) \longleftrightarrow \Phi, \quad \nabla a(t,\mathbf{x}) \longleftrightarrow -\mathbf{E}$

NMR-induced Axion

In electrodynamics: $\rho_{\rm p} = -\nabla \cdot \mathbf{P}$

- **Coherent spin-precessing source:**

$$a(t,\mathbf{x}) = g_{aN} \int d^3x' \, \frac{1}{4\pi|\mathbf{x}-\mathbf{x}'|} e^{ik_0|\mathbf{x}-\mathbf{x}'|} \rho_{\rm s}(t,\mathbf{x}')$$

$\rho_{\rm s}(t,\mathbf{x}) \equiv -2\nabla \cdot \mathbf{s}(t,\mathbf{x})$

A "spin charge" distribution induced by spin polarization

$$k_0 \equiv \begin{cases} \sqrt{\omega_0^2 - m_a^2}, & (\text{if } \omega_0 \geq m_a) \\ i\kappa_0, \ \kappa_0 \equiv \sqrt{m_a^2 - \omega_0^2} & (\text{if } \omega_0 < m_a) \end{cases}$$

$$\mathbf{s}(t,\mathbf{x}) = e^{-i\omega_0 t}\mathbf{s}(\mathbf{x}), \quad \rho_{\rm s}(t,\mathbf{x}) = e^{-i\omega_0 t}\rho_{\rm s}(\mathbf{x}), \quad a(t,\mathbf{x}) = e^{-i\omega_0 t}a(\mathbf{x})$$ (Real part as the physical quantity)

- **Near-Field Limit:** $k_0|\mathbf{x}-\mathbf{x}'| \ll 1$ or $\kappa_0|\mathbf{x}-\mathbf{x}'| \ll 1$ $\qquad 1\text{GHz} \times 1\text{cm} \simeq 0.03$

$$a(t,\mathbf{x}) = g_{aN} \int d^3x' \, \frac{1}{4\pi|\mathbf{x}-\mathbf{x}'|} \rho_{\rm s}(t,\mathbf{x}'), \qquad \nabla a(t,\mathbf{x}) = -g_{aN} \int d^3x' \, \frac{\mathbf{x}-\mathbf{x}'}{4\pi|\mathbf{x}-\mathbf{x}'|^3} \rho_{\rm s}(t,\mathbf{x}')$$

Analogy with electrostatics

$g_{aN} \longleftrightarrow 1/\epsilon_0, \quad a(t,\mathbf{x}) \longleftrightarrow \Phi, \quad \nabla a(t,\mathbf{x}) \longleftrightarrow -\mathbf{E}$

"The Spin Charge Picture"

Axion Field Configuration

$$\rho_s(t,\mathbf{x}) \equiv -2\nabla\cdot\mathbf{s}(t,\mathbf{x})$$

$$\nabla a(t,\mathbf{x}) \longleftrightarrow -\mathbf{E}$$

- **Uniform Source Material with Spins in Alignment:**

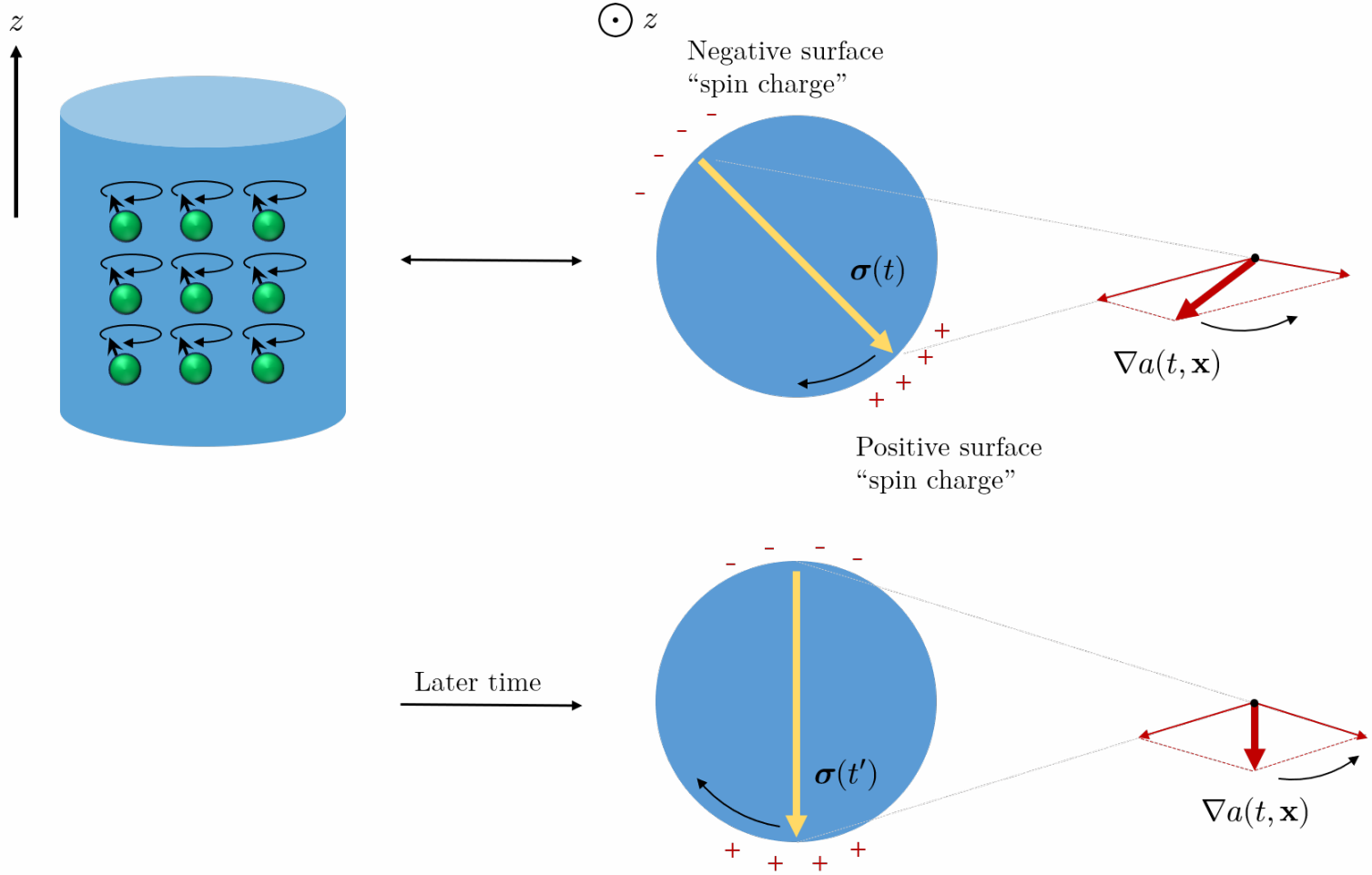

Axion-induced NMR

$$\mathbf{B}_a(t,\mathbf{x}) = \frac{2g_{aN}}{\gamma}\nabla a(t,\mathbf{x})$$

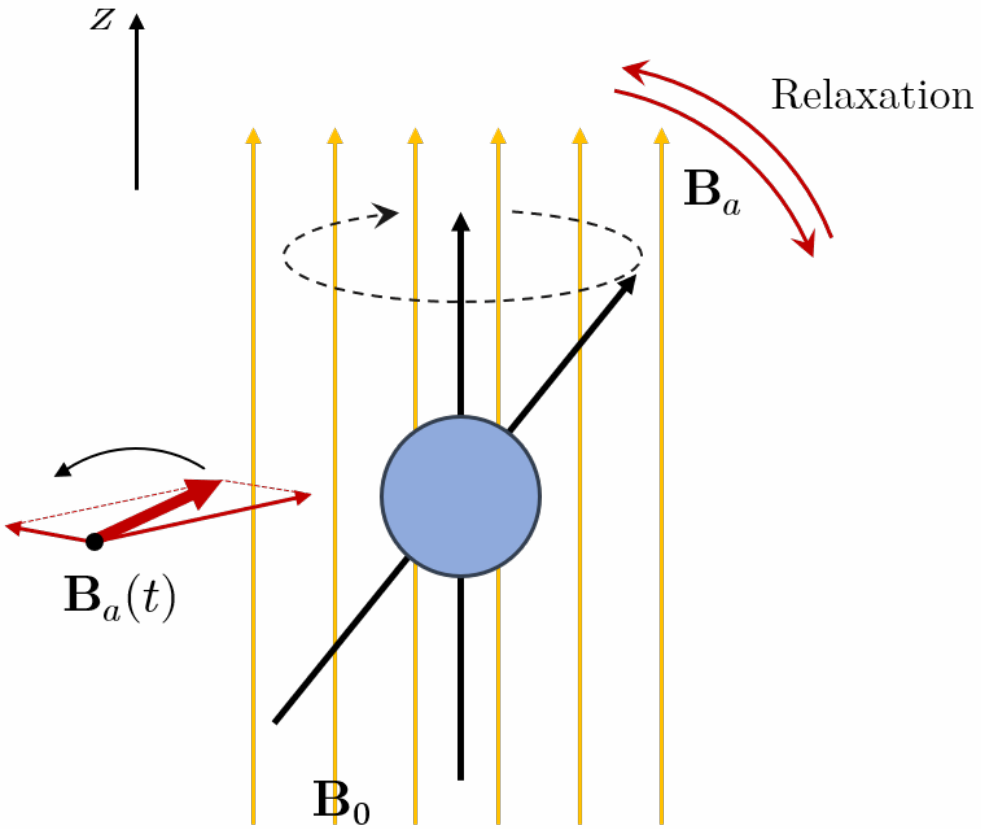

Axion-induced NMR

$$\mathbf{B}_a(t,\mathbf{x}) = \frac{2g_{aN}}{\gamma}\nabla a(t,\mathbf{x})$$

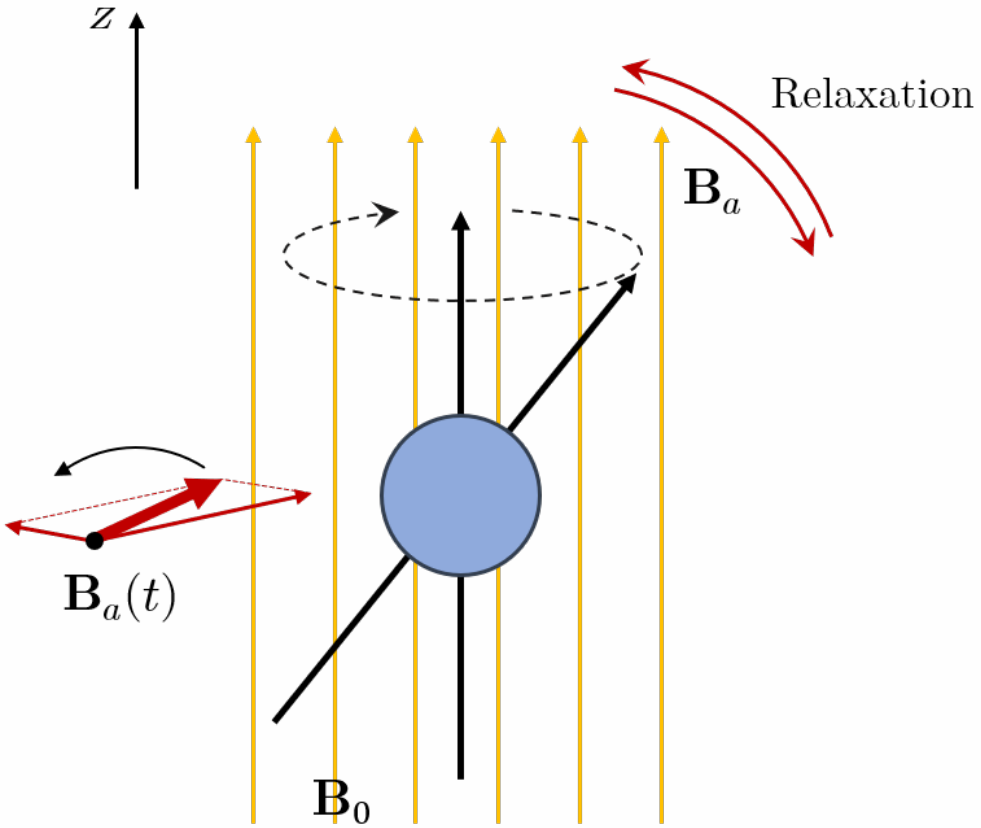

On resonance, axion turned on at t=0:

$$M_x(t,\mathbf{x}) \simeq -g_{aN}M_0T_2|\mathcal{A}(\mathbf{x})|\left(1-e^{-t/T_2}\right)\sin\left(\omega_0 t+\varphi(\mathbf{x})\right)$$

Transverses relaxation time

$$\mathcal{A}(\mathbf{x}) \equiv \pm\partial_x a(\mathbf{x}) + i\partial_y a(\mathbf{x}) \qquad (+ \text{ for } \gamma>0,\ - \text{ for } \gamma<0)$$

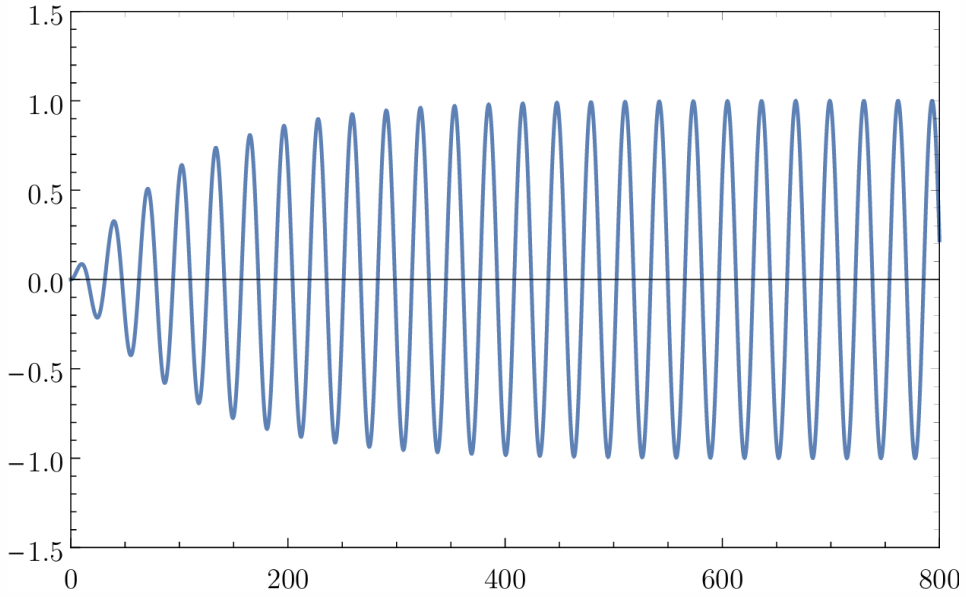

Dual NMR Setup

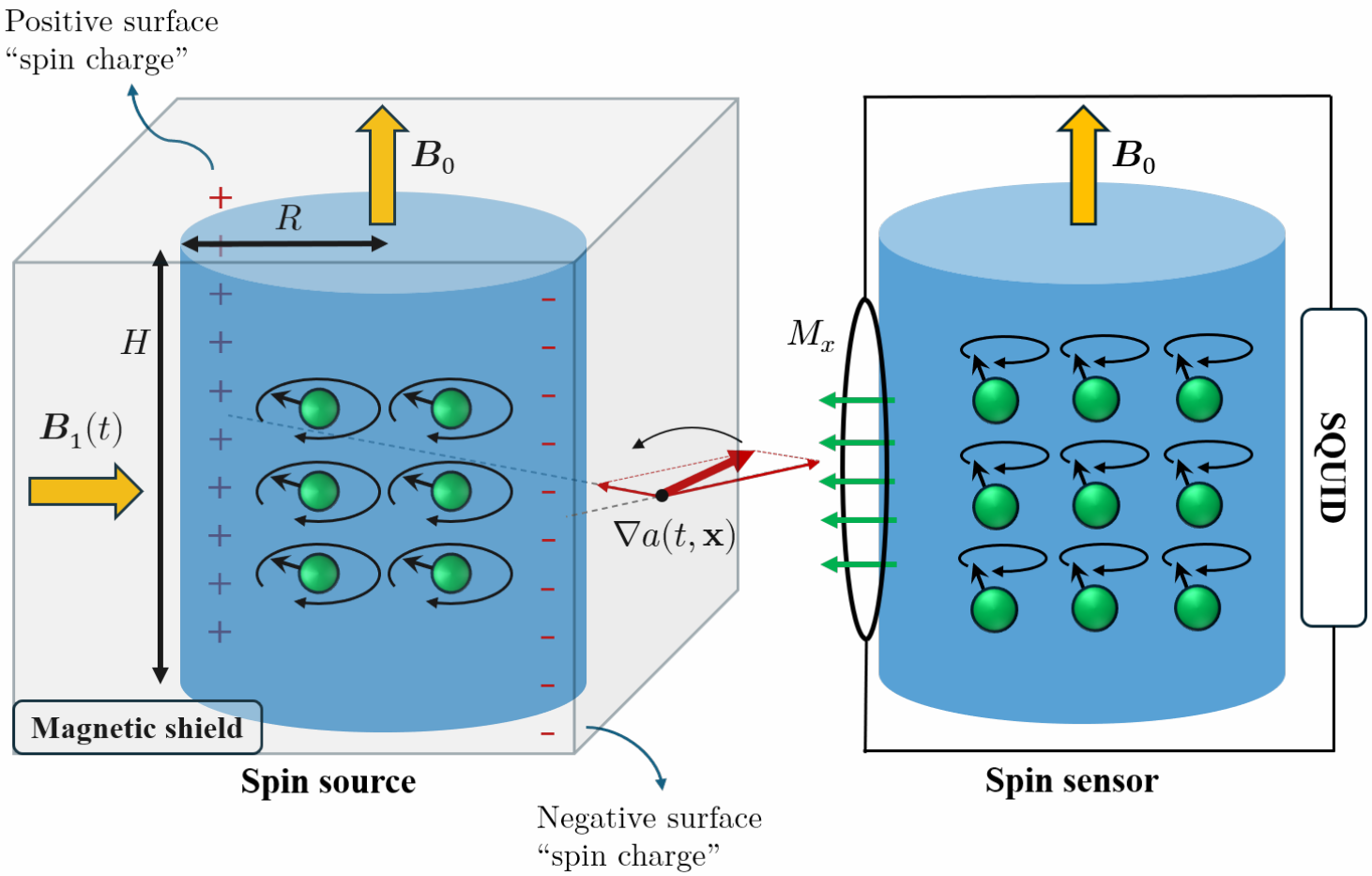

SQUID magnetometer: senses magnetic fluxes in the pickup loop

Noise Sources

- **Thermal Noise**
  - Cool down the apparatus
- **Spin-projection Noise:** $\langle\uparrow| S_x(t)S_x(t') |\uparrow\rangle \neq 0$
- **SQUID Noise:** Sensitivity limit of the magnetometer
- **Contamination**: $\mathbf{B}_1$ that drives the NMR in the source
  - Magnetic shielding

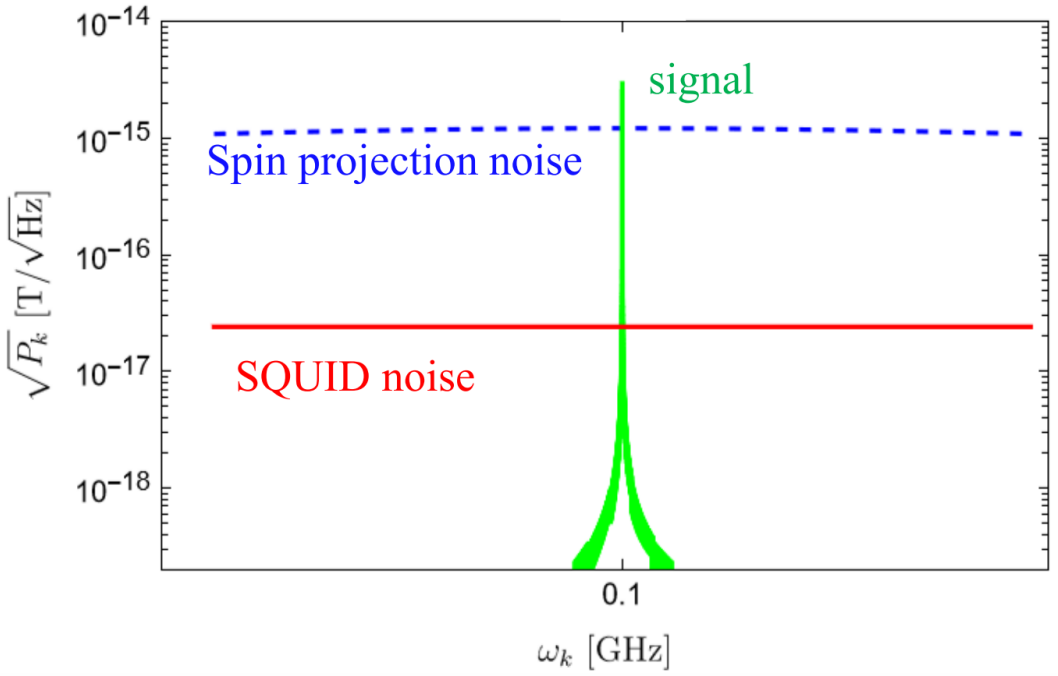

$$\omega_0 R \simeq 0.25 \left(\frac{B_0}{10\mathrm{T}}\right)\left(\frac{R}{10\mathrm{cm}}\right)$$

Near-field (almost)

$B_0 = 10\mathrm{T} \implies \omega_0 = 0.74\,\mathrm{GHz}$

Distance $= R$

$^{129}\mathrm{Xe}:\quad n_N = 1.3 \times 10^{22}\,\mathrm{cm}^{-3}$

$\gamma = -7.40 \times 10^7\,\mathrm{s}^{-1}\mathrm{T}^{-1}$

$T_2 = 100\mathrm{s}$

hyperpolarized

$R = 0.1,\ 1,\ 5,\ 10$ cm

fix $H/R = 3$

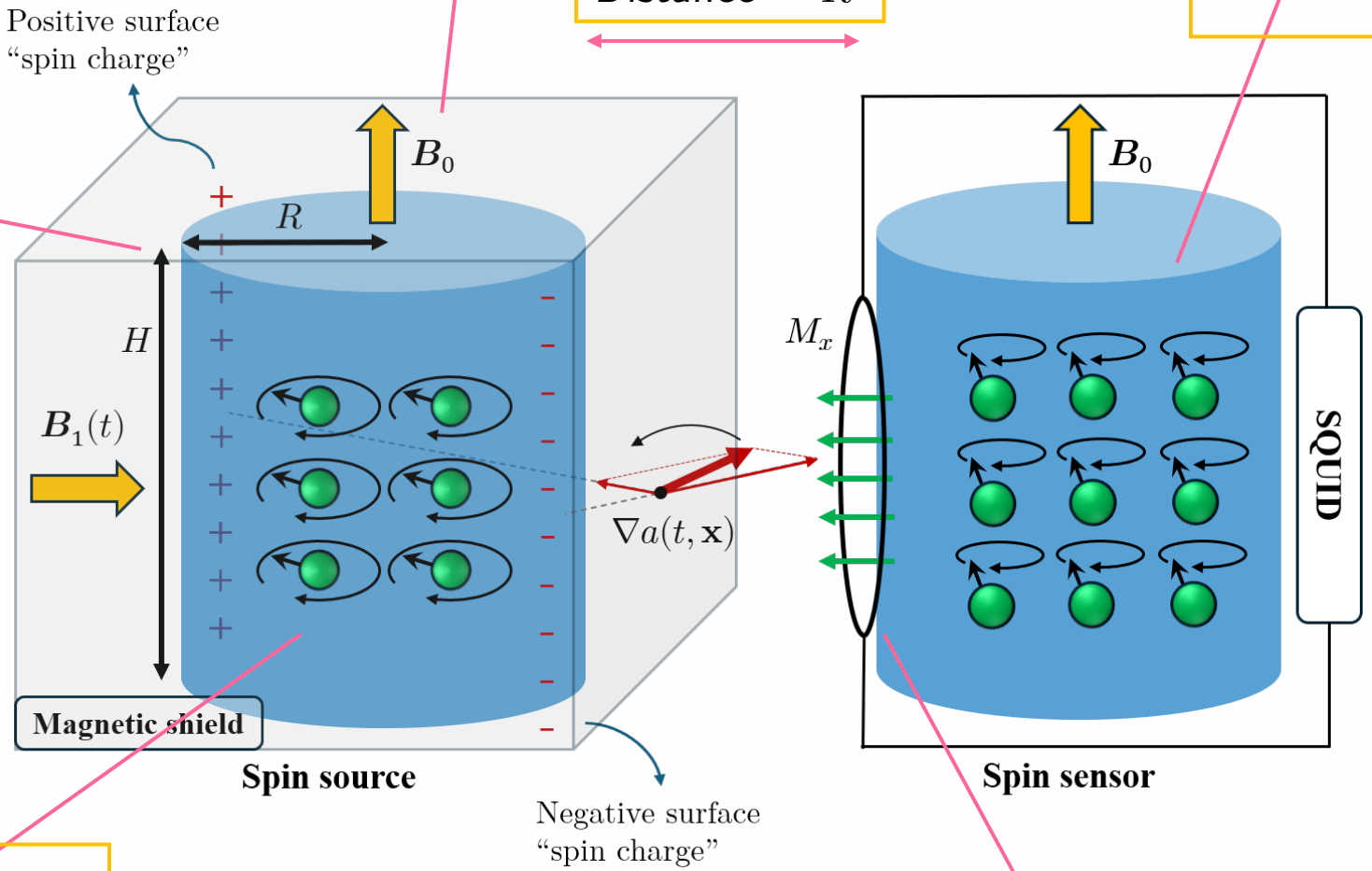

Maintain a 90° tilt

Placed at the near end

Benchmark Sensitivities

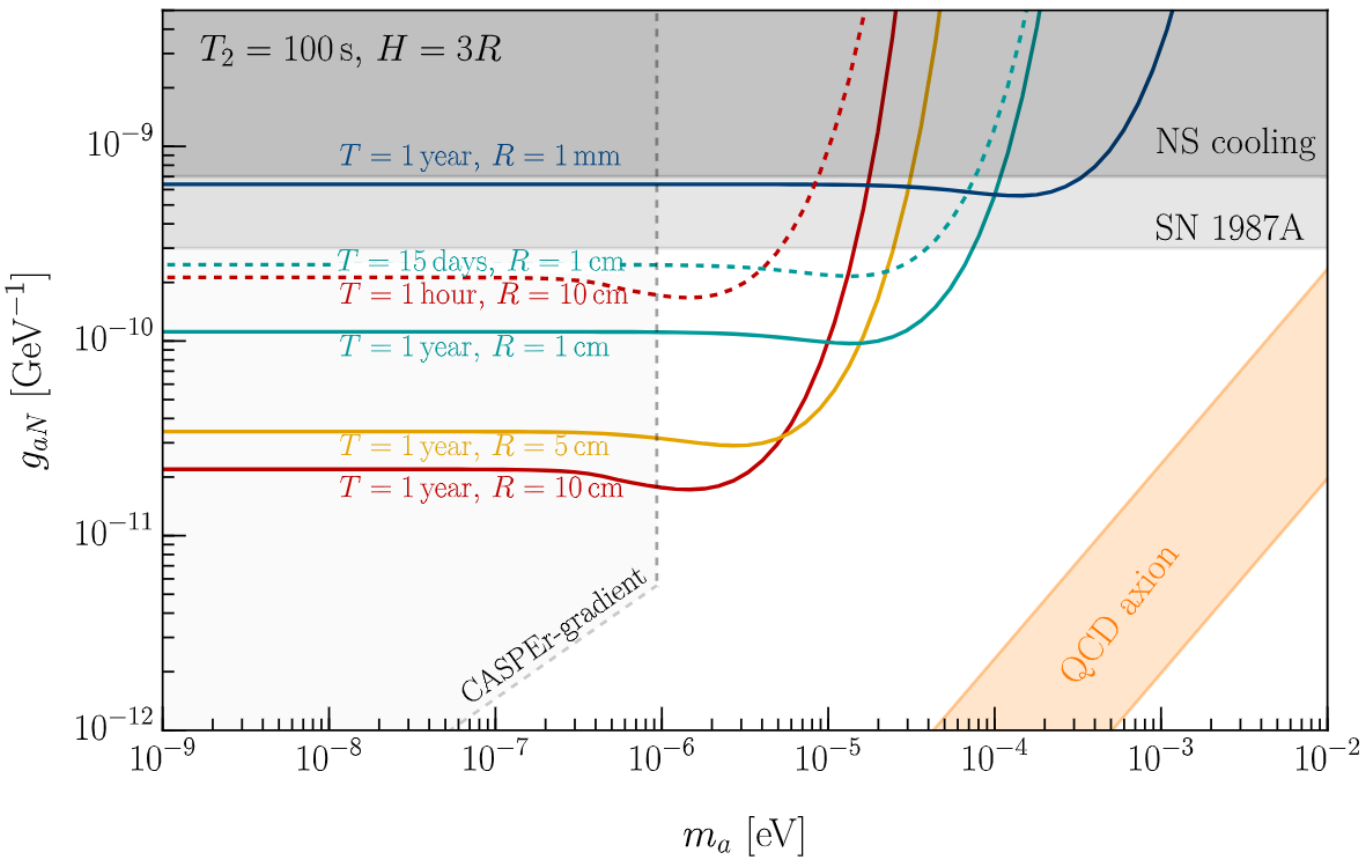

Benchmark Sensitivities

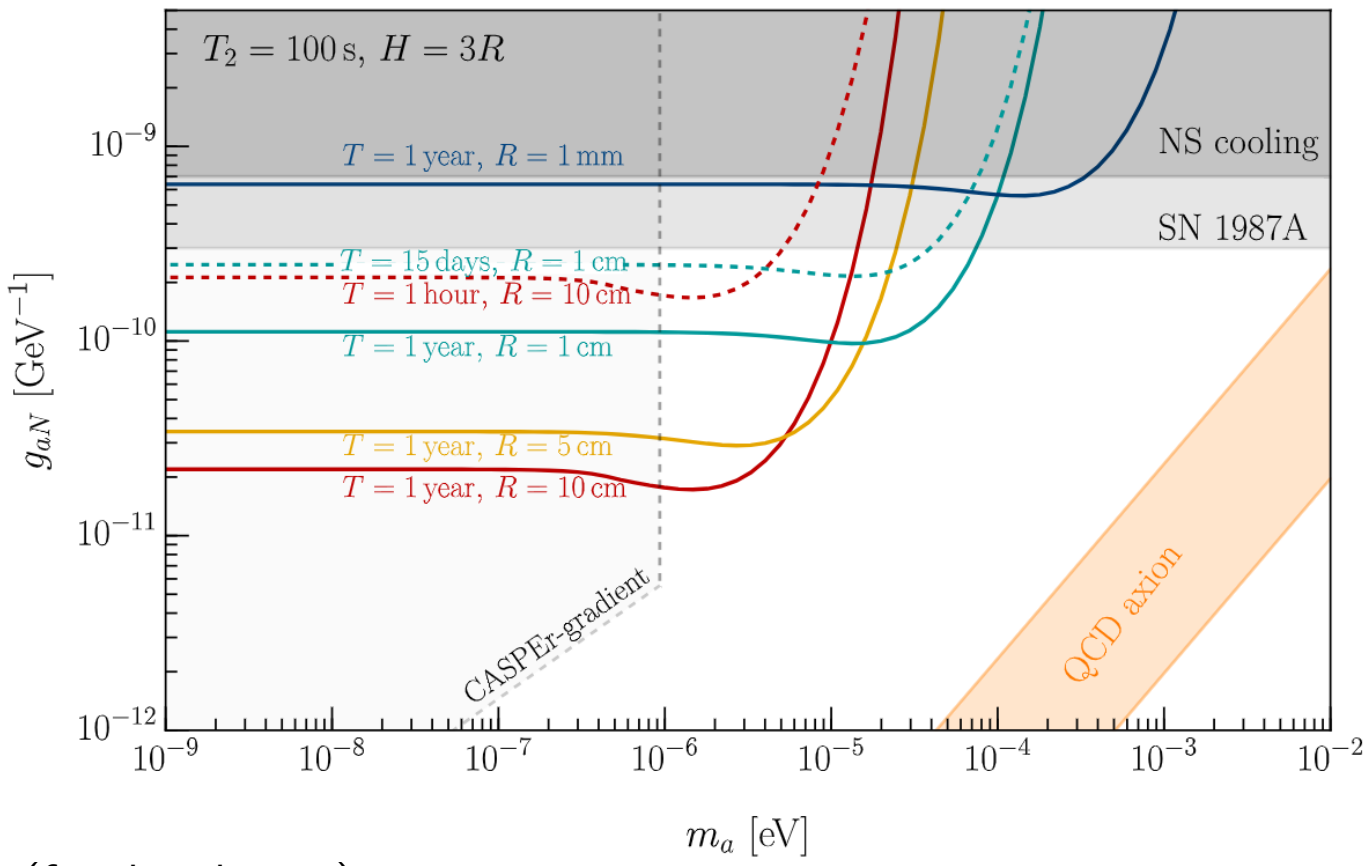

- Scaling relation (for the plateau):

Volume of detection sample

$$g_{aN}^{(95\%)} \simeq 2 \times 10^{-11}\,\mathrm{GeV}^{-1} \left(\frac{n_N}{1.3 \times 10^{22}\,\mathrm{cm}^{-3}}\right)^{-3/4} \left(\frac{T_2}{100\,\mathrm{s}}\right)^{-1/4} \left(\frac{T}{1\,\mathrm{yr}}\right)^{-1/4} \left(\frac{V}{0.01\,\mathrm{m}^3}\right)^{-1/4}$$

Highlights

Advantage #1: Relying only on the axion-nucleon coupling, no assumption of axion dark matter

Highlights

Advantage #1: Relying only on the axion-nucleon coupling, no assumption of axion dark matter

Advantage #2: Highly coherent axion field, oscillating at the spin precession frequency of the source

→ ① Broad-band axion search with a single frequency for long durations
② Precise frequency matching between the axion field and the sensor

Highlights

Advantage #1: Relying only on the axion-nucleon coupling, no assumption of axion dark matter

Advantage #2: Highly coherent axion field, oscillating at the spin precession frequency of the source

→
① Broad-band axion search with a single frequency for long durations
② Precise frequency matching between the axion field and the sensor

Advantage #3: Gradient enhanced by spatial inhomogeneity: $\left|\frac{\partial_x a}{a}\right| \sim \frac{1}{R}$

Highlights

Advantage #1: Relying only on the axion-nucleon coupling, no assumption of axion dark matter

Advantage #2: Highly coherent axion field, oscillating at the spin precession frequency of the source

→ ① Broad-band axion search with a single frequency for long durations
② Precise frequency matching between the axion field and the sensor

Advantage #3: Gradient enhanced by spatial inhomogeneity: $\left|\frac{\partial_x a}{a}\right| \sim \frac{1}{R}$

Advantage #4: Capable of probing a larger mass range: $m_a \sim \frac{1}{R}$

Highlights

Advantage #1: Relying only on the axion-nucleon coupling, no assumption of axion dark matter

Advantage #2: Highly coherent axion field, oscillating at the spin precession frequency of the source

→ ① Broad-band axion search with a single frequency for long durations
② Precise frequency matching between the axion field and the sensor

Advantage #3: Gradient enhanced by spatial inhomogeneity: $\left|\frac{\partial_x a}{a}\right| \sim \frac{1}{R}$

Advantage #4: Capable of probing a larger mass range: $m_a \sim \frac{1}{R}$

Advantage #5: Achievable with centimeter-scale devices [LSTWs: $O(100)$m]

Highlights

Advantage #1: Relying only on the axion-nucleon coupling, no assumption of axion dark matter

Advantage #2: Highly coherent axion field, oscillating at the spin precession frequency of the source

→ ① Broad-band axion search with a single frequency for long durations
② Precise frequency matching between the axion field and the sensor

Advantage #3: Gradient enhanced by spatial inhomogeneity: $\left|\frac{\partial_x a}{a}\right| \sim \frac{1}{R}$

Advantage #4: Capable of probing a larger mass range: $m_a \sim \frac{1}{R}$

Advantage #5: Achievable with centimeter-scale devices [LSTWs: $O(100)$m]

Advantage #6: Can be split into multiple experiments without loss of sensitivity

→ ① Regular power on/off and calibration
② Multiple experiments at the same time

Conclusion

- **Dual NMR:** compelling sensitivity to axions through the axion-nucleon coupling

Design: QW
Production: ChatGPT

Backup Slides

B1. Axion-nucleon/nucleus Coupling

Operator $g_{aN}\mathbf{I}$ and $g_{ap}\mathbf{S}_p + g_{an}\mathbf{S}_n$ should be the same in the Hilbert space of a non-relativistic nucleus.

$\mathbf{I}$: nucleus spin $\qquad \mathbf{S}_p \equiv \sum_{k=1}^{Z} \mathbf{S}_{p_k}$: total proton spin $\qquad \mathbf{S}_n \equiv \sum_{l=1}^{N} \mathbf{S}_{n_l}$: total neutron spin

Define $\langle ... \rangle \equiv \langle \alpha, i, i_z | \, ... \, | \alpha, i, i_z \rangle \quad \Longrightarrow \quad \langle g_{aN}\mathbf{I} \rangle = \langle g_{ap}\mathbf{S}_p \rangle + \langle g_{an}\mathbf{S}_n \rangle$

z component:

$$g_{aN} = g_{ap}\frac{\langle S_{pz} \rangle}{i_z} + g_{an}\frac{\langle S_{nz} \rangle}{i_z}$$

For $^{129}\mathrm{Xe}$: $\quad i_z = \frac{1}{2}, \quad \langle S_{pz} \rangle \simeq 0.023, \quad \langle S_{pn} \rangle \simeq 0.300 \quad \Longrightarrow \quad g_{aN} \simeq 0.046\, g_{ap} + 0.600\, g_{an}$

[Stadnik, et al. – 2014]

Single-particle approximation (Schimidt model):

[Krane – 1955, p.604]

For nuclear ground states, there are several rules for determining the spins:

1. All even-Z, even-N nuclei have $I = 0$. This results from the strong tendency of nucleons to couple pairwise to zero spin.
2. In odd-A nuclei, the net spin is almost always determined by the j of the last odd particle, with the remaining $A - 1$ nucleons (having even numbers of protons and neutrons) pairing to zero spin as above.
3. In odd-Z, odd-N nuclei, the spin is determined by the vector coupling of the j of the odd proton and neutron, $\boldsymbol{I} = \boldsymbol{j}_p + \boldsymbol{j}_n$, and thus any of several values are possible. To determine which of these possible couplings will be the ground state, we use the empirical rule that the ground state is usually the coupling with the neutron and proton intrinsic spins $\boldsymbol{s}_p$ and $\boldsymbol{s}_n$ parallel. As an example, consider ^{38}Cl, which consists of a $d_{3/2}$ proton coupled to an $f_{7/2}$ neutron. For the proton, $\ell_p = 2$ and thus $\boldsymbol{s}_p$ is opposite to $\boldsymbol{j}_p$. For the neutron, $\ell_n = 3$ and $\boldsymbol{s}_n$ is parallel to $\boldsymbol{j}_n$. Arranging the coupling so that $\boldsymbol{s}_p$ and $\boldsymbol{s}_n$ are parallel, as in Figure 16.1, we get $I = |j_p - j_n|$ or $I = 2$, which is in fact the ground-state spin of ^{38}Cl. (The first excited state is $I = 5$, corresponding to $I = j_p + j_n$.) On the other hand, consider ^{50}Sc, resulting from an $f_{7/2}$ proton coupled to a $p_{3/2}$ neutron. Here making $\boldsymbol{s}_p$ and $\boldsymbol{s}_n$

B2. Benchmark Field Magnitudes

- Cylindrical, $H/R = 3$
- $\mathbf{B}_0$ static, $\mathbf{B}_1$ alternating
- $\omega_0 = |\gamma B_0|$ (Larmor frequency)
- Hyperpolarized
- 90° tilt

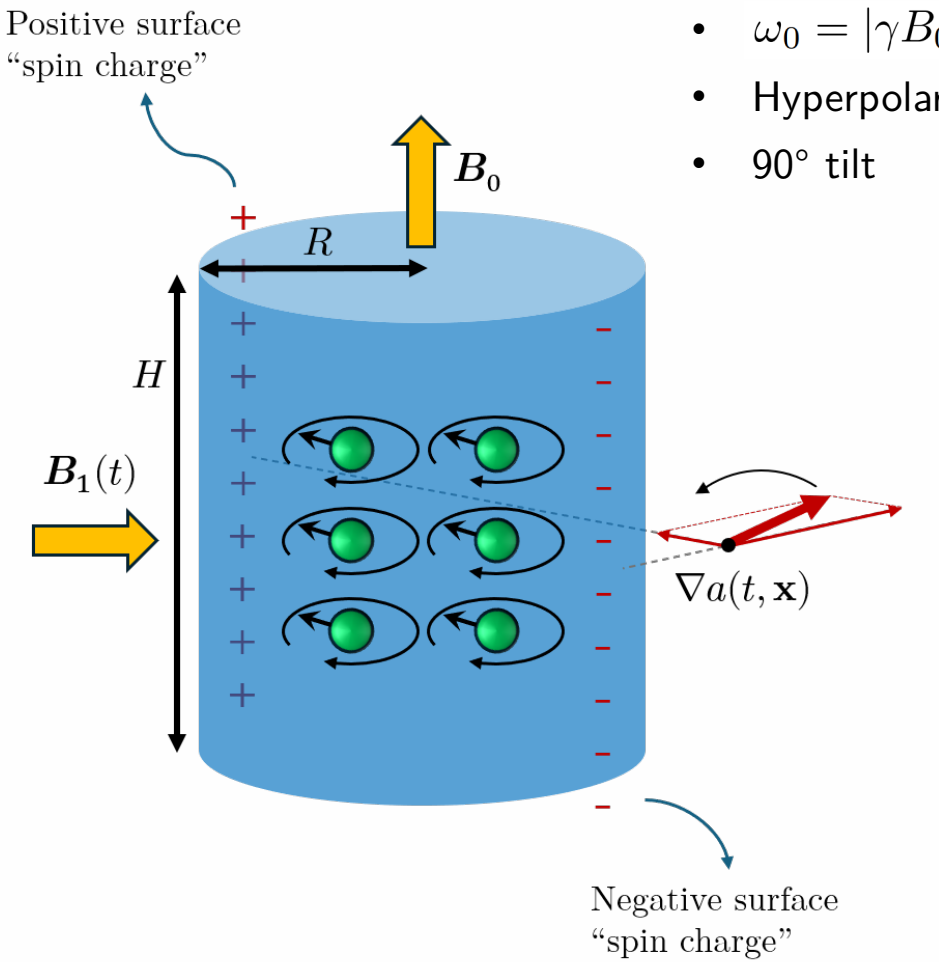

Axion dark matter:

$$\rho_{\rm DM} \simeq 0.3 {\rm GeV/cm}^3, \quad v_0 \sim 10^{-3}$$

$$a = \sqrt{2\rho_{\rm DM}}/m_a \sim 10^3 {\rm eV} \left(\frac{m_a}{1\mu{\rm eV}}\right)^{-1}$$

$$|\nabla a| \sim m_a v_0 a_0 \sim 10^{-6} {\rm eV}^2$$

$$\left|\frac{\nabla a}{a}\right| \sim m_a v_0 \sim 10^{-9} {\rm eV} \left(\frac{m_a}{1\mu{\rm eV}}\right)$$

Near-zone field amplitude: (origin at cylinder center)

$$a(x\hat{\mathbf{x}}) \simeq 2.4\,\mu{\rm eV} \left(\frac{x}{R}\right)^{-1.6} \left(\frac{g_{aN}}{10^{-10}\ {\rm GeV}^{-1}}\right) \left(\frac{n_N}{1.3\times 10^{22}\,{\rm cm}^{-3}}\right) \left(\frac{R}{10\ {\rm cm}}\right),$$

$$\partial_x a(x\hat{\mathbf{x}}) \simeq -7.6\,\mu{\rm eV}^2 \left(\frac{x}{R}\right)^{-2.6} \left(\frac{g_{aN}}{10^{-10}{\rm GeV}^{-1}}\right) \left(\frac{n_N}{1.3\times 10^{22}\,{\rm cm}^{-3}}\right).$$

$$\left|\frac{\partial_x a}{a}\right| \sim \frac{1}{R} \sim 1\ \mu{\rm eV} \left(\frac{R}{10\ {\rm cm}}\right)^{-1}$$

B3. Power Spectrum Density (PSD)

$$\omega_k \equiv 2\pi k/T, \quad \Delta\omega_k \equiv \omega_k - \omega_0$$

Signal PSD:

$$P_k^a(\mathbf{x}) \simeq \frac{g_{aN}^2 M_0^2 T_2^2 |\mathcal{A}(\mathbf{x})|^2}{\Delta\omega_k^2 T} \sin^2\left[\frac{1}{2}\Delta\omega_k T\right]$$

$\propto T \times$

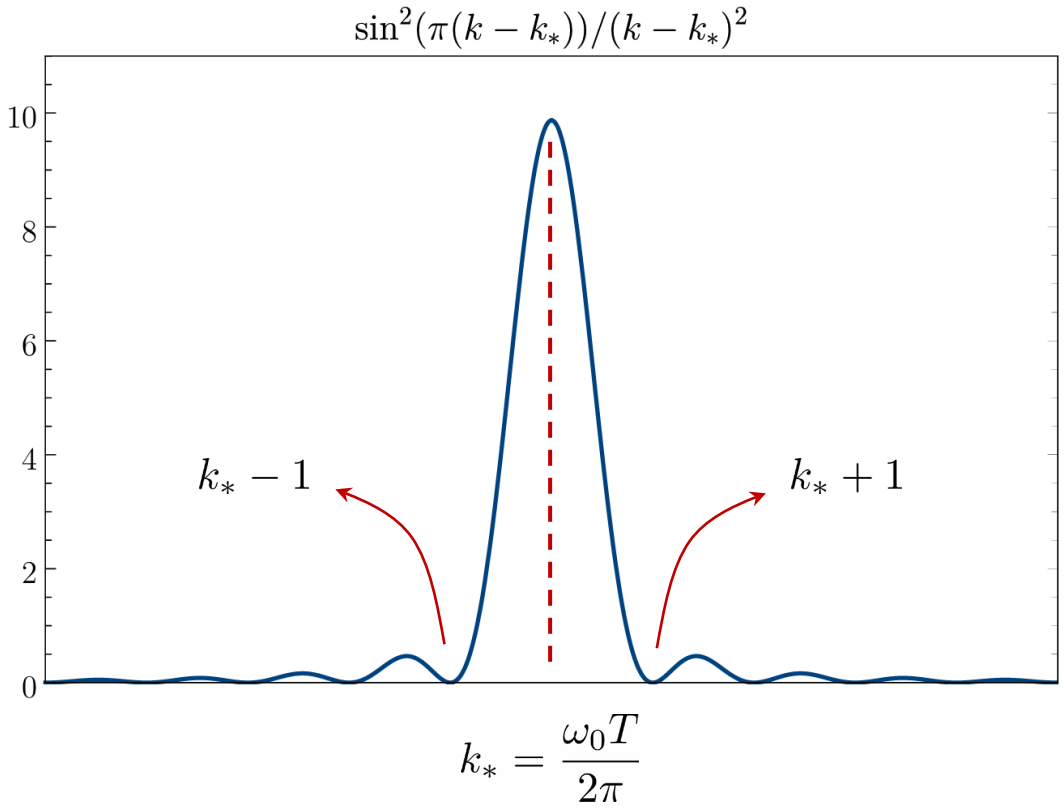

Noise PSD:

- **Spin-projection Noise:** $\langle\uparrow| S_x(t)S_x(t')|\uparrow\rangle \neq 0$

$$P_k^{\mathrm{SP}} = \frac{\gamma^2 n_N J}{2V}\frac{T_2}{1+\Delta\omega_k^2 T_2^2}$$ [Dror, et al. – 2022]

- **SQUID Noise:**

[CASPEr – 2013, Dror, et al. – 2022]

$$P_k^{\mathrm{SQ}} = \frac{1}{A_{\mathrm{eff}}^2}P_{\Phi\Phi}^{\mathrm{SQ}}, \quad P_{\Phi\Phi}^{\mathrm{SQ}} \simeq (10^{-7}\Phi_0)^2/\mathrm{Hz}, \quad A_{\mathrm{eff}} \simeq 0.3\,\mathrm{cm}^2\left(\frac{A}{80\,\mathrm{cm}^2}\right)$$

B4. Scaling Relation

The signal lies predominantly in a single bin $k_* = \omega_0 T/2\pi$ ⟹ $\mathrm{SNR} = \dfrac{P^a_{k_*}}{B_{k_*}}, \quad B_{k_*} = P^{\mathrm{SQ}}_{k_*} + P^{\mathrm{SP}}_{k_*} \simeq P^{\mathrm{SP}}_{k_*}$

Setting SNR to a constant threshold:

Volume of detection sample

$$g_{aN} \propto n_N^{-3/4} T_2^{-1/4} T^{-1/4} V^{-1/4} |\mathcal{G}(\mathbf{x}_0)|^{-1/2}$$

At the pick-up loop

$$\mathcal{G}(\mathbf{x}) \equiv \frac{\mathcal{A}(\mathbf{x})}{g_{aN} n_N}$$

A dimensionless **driving force** that encapsulates factors from the production side, only depending on ω_0, m_a and the geometry of the source sample

Plateau region: near-field value $|\mathcal{G}(\mathbf{x}_0)| \simeq 0.05, \quad \mathbf{x}_0 = (2R, 0, 0)$

$$g_{aN}^{(\mathrm{UL})} \simeq 2 \times 10^{-11}\,\mathrm{GeV}^{-1} \left(\frac{n_N}{1.3 \times 10^{22}\,\mathrm{cm}^{-3}}\right)^{-3/4} \left(\frac{T_2}{100\,\mathrm{s}}\right)^{-1/4} \left(\frac{T}{1\,\mathrm{yr}}\right)^{-1/4} \left(\frac{V}{0.01\,\mathrm{m}^3}\right)^{-1/4}$$

B5. Driving Force Function $\mathcal{G}(\mathbf{x})$

$$\mathcal{G}(\mathbf{x}) \equiv \frac{\mathcal{A}(\mathbf{x})}{g_{aN} n_N}, \qquad \mathcal{A}(\mathbf{x}) \equiv \pm \partial_x a(\mathbf{x}) + i \partial_y a(\mathbf{x}) \quad (+ \text{ for } \gamma > 0, - \text{ for } \gamma < 0)$$

- Plug in $a(t, \mathbf{x}) = g_{aN} \int d^3x' \, \frac{1}{4\pi |\mathbf{x} - \mathbf{x}'|} e^{i k_0 |\mathbf{x} - \mathbf{x}'|} \, \rho_{\mathrm{s}}(t, \mathbf{x}')$ (origin fixed at source cylinder center)
- Take $\boldsymbol{\sigma}(t) = e^{-i\omega_0 t}(\hat{\mathbf{x}} \mp i\hat{\mathbf{y}}), \quad (- \text{ for } \gamma > 0, \; + \text{ for } \gamma < 0)$

  CW **CCW** (viewed from above, with $\mathbf{B}_0$ in $+z$ direction)
- Define dimensionless quantities: $\tilde{\mathbf{x}} \equiv \mathbf{x}/R, \quad \tilde{\mathbf{x}}' \equiv \mathbf{x}'/R$

$$\mathcal{G}(\mathbf{x}) = \mp \int_{\text{Source}} d^3\tilde{x}' \left(\partial_{\tilde{x}}^2 + \partial_{\tilde{y}}^2\right) \left(\frac{1}{4\pi |\tilde{\mathbf{x}} - \tilde{\mathbf{x}}'|} e^{i k_0 R |\tilde{\mathbf{x}} - \tilde{\mathbf{x}}'|} \right), \quad (- \text{ for } \gamma > 0, \; + \text{ for } \gamma < 0)$$

⇒ **Only depends on $k_0 R$, H/R, and $\mathbf{x}/R$**

Source-Geometrical Dependence:

Near-field limit (plateau region): $k_0 R \ll 1$ or $\kappa_0 R \ll 1$

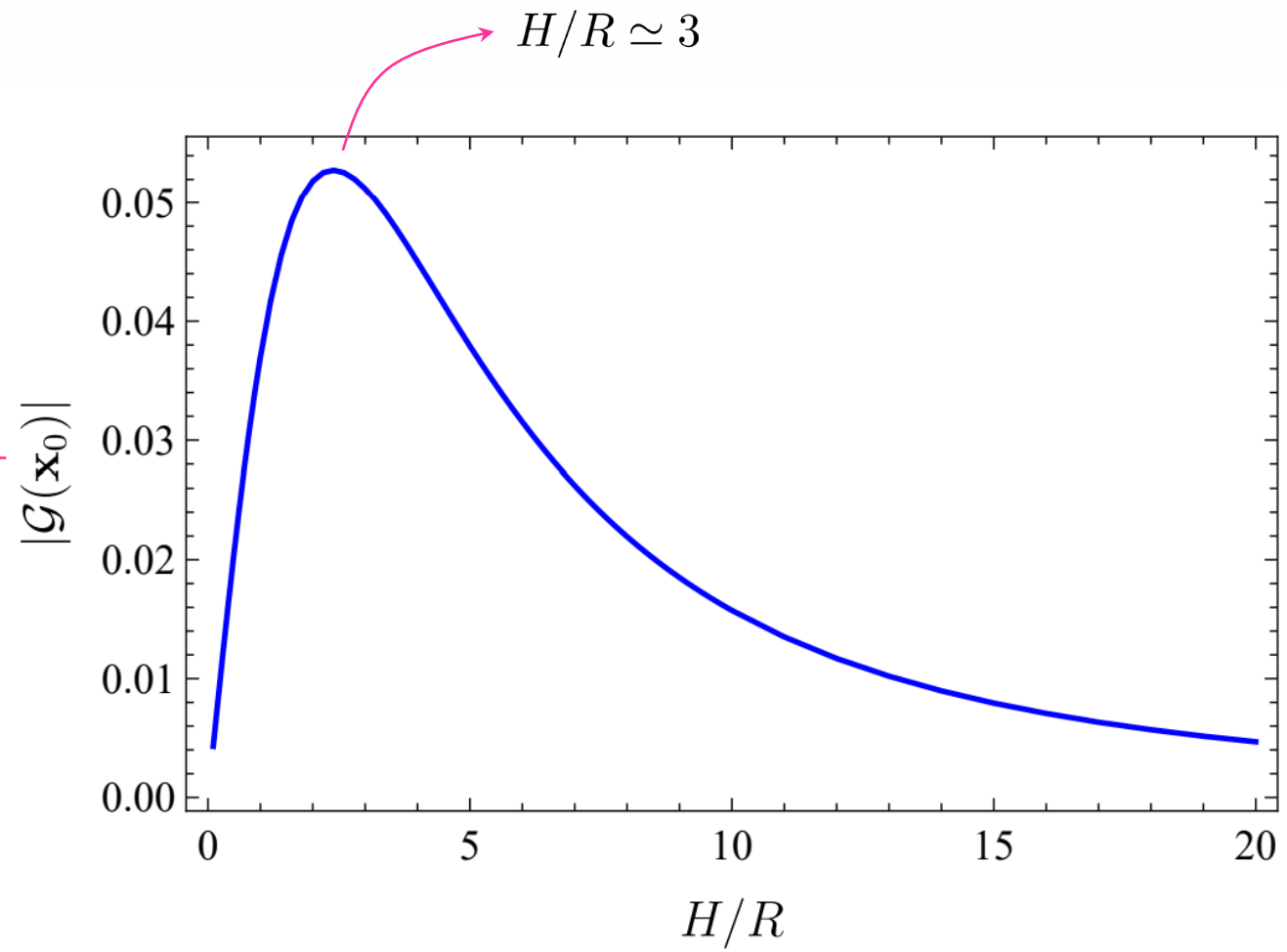

$\mathbf{x}_0 = (2R, 0, 0)$

at the pickup loop (near end)

Frequency and Mass Dependence:

$\mathbf{x}_0 = (2R, 0, 0)$ at the pickup loop (near end)

Height-to-radius ratio $H/R \simeq 3$

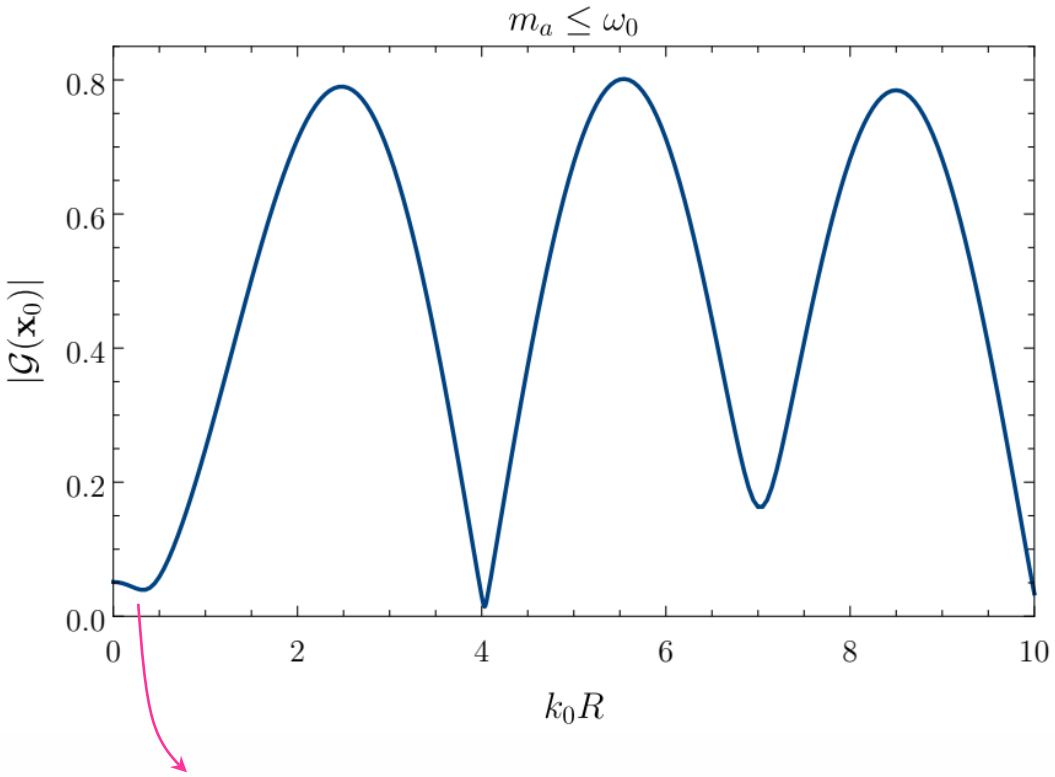

Maximal detectable mass $\kappa_0 R \simeq 0.7$

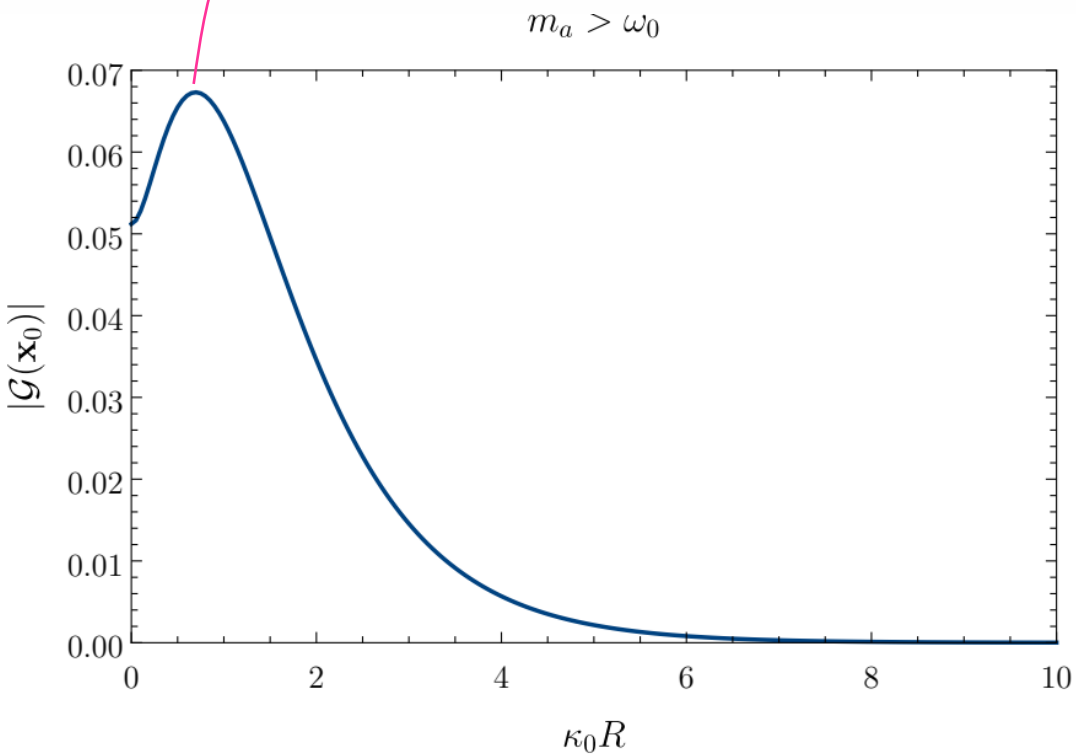

The plateau region in our projections $k_0 R \simeq \omega_0 R \ll 1$

B6. Magnetization-induced Magnetic field

$$\mathbf{M}_{xy} \implies B_x \implies \text{sensed by the SQUID pick-up coil}$$

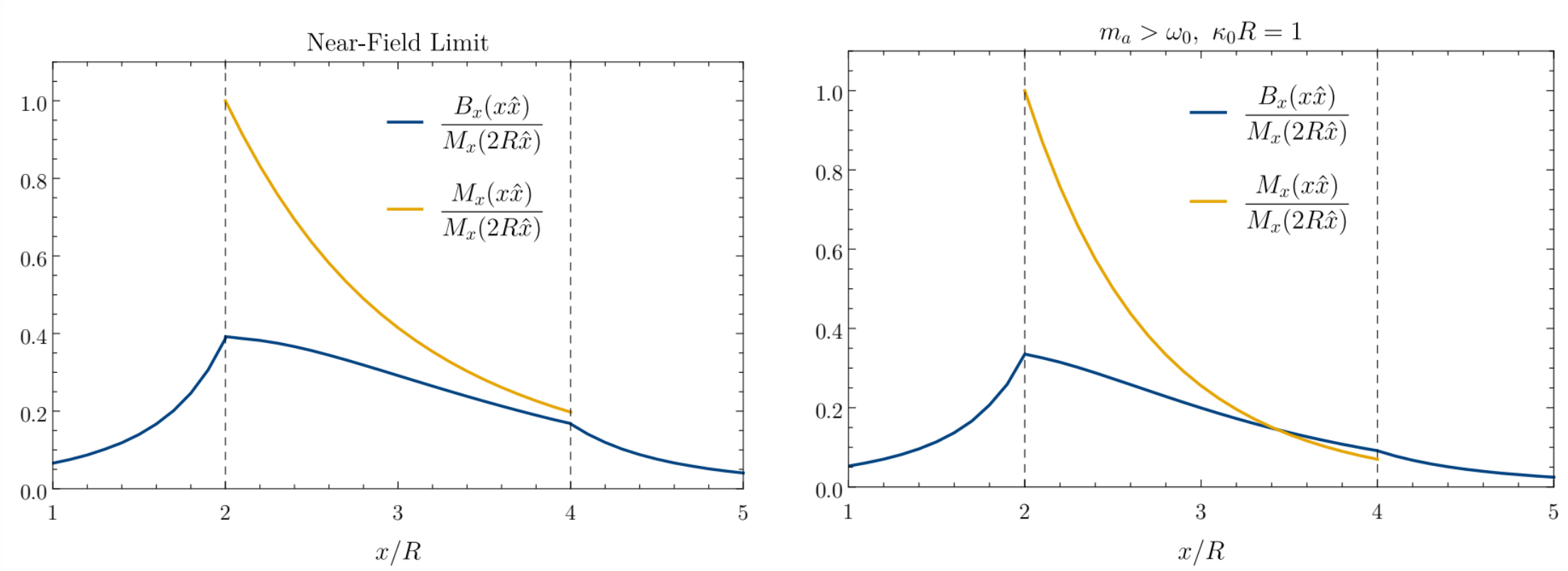

B_x maximized at the near end $\mathbf{x}_0 = (2R, 0, 0)$, with $B_x(\mathbf{x}_0) = \mathcal{O}(1)\, M_x(\mathbf{x}_0)$